Dalton Transactions



PAPER View Article Online
View Journal | View Issue



Cite this: *Dalton Trans.*, 2022, **51**, 8688

Received 19th April 2022, Accepted 16th May 2022 DOI: 10.1039/d2dt01224c

rsc.li/dalton

The non-centrosymmetric layered compounds IrTe₂I and RhTe₂I†

Danrui Ni, ¹ a Xin Gui, ¹ a Bingzheng Han, ^b Haozhe Wang, ¹ and Robert J. Cava*^a

The previously unreported layered compounds $IrTe_2I$ and $RhTe_2I$ were prepared by a high-pressure synthesis method. Single crystal X-ray and powder X-ray diffraction studies find that the compounds are isostructural, crystallizing in a layered orthorhombic structure in the non-centrosymmetric, non-symmorphic space group $Pca2_1$ (#29). Characterization reveals diamagnetic, high resistivity, semiconducting behavior for both compounds, consistent with the +3 chemical valence and d^6 electronic configurations for both iridium and rhodium and the Te-Te dimers seen in the structural study. Electronic band structures are calculated for both compounds, showing good agreement with the experimental results.

1. Introduction

Inorganic heavy metal compounds based on halogens and/or chalcogens have been studied for decades due to their electronic and magnetic properties and multiple potential applications. This family includes thermoelectric materials, 1-3 applications in photovoltaic devices^{4,5} and radiation detectors,^{6,7} and quantum materials⁸⁻¹¹ for example. Especially of recent interest have been heavy transition metal chalcogenides or halides with layered crystal structures, as their resulting pseudo 2D electronic and magnetic systems, together with the van der Waals forces between the layers, provide both a platform for studying forefront spin/electron interactions, and for further fabrication and modification. 12-15 In recent years, many lavered compounds containing Group VIII elements (such as ruthenium, rhodium, and iridium), are of great research interest, and have been studied as candidates for quantum spin liquids, topological insulators, and superconductors. 16-19

In this report, we describe layered IrTe₂I and RhTe₂I, prepared by a high-pressure solid-state method. These compounds have not been reported previously, and do not appear to form using an ambient pressure high temperature synthesis method. With the help of high pressure, which often results in denser phases, uncommon structural features, and some pressure-induced properties, ^{20–23} we find that these materials crystallize in a new layered structure. The structure is refined in the *Pca*2₁

space group, which is both nonsymmorphic and noncentrosymmetric, by single crystal and powder X-ray diffraction. Te–Te bonding is found in the structure, which is consistent with the d^6 configuration of Rh(III) and Ir(III), and the diamagnetic behavior and high resistivities of the compounds. Both experimental results and theoretical calculations suggest a semiconducting nature for the two compounds. Their non-centrosymmetric, non-symmorphic layered structure may trigger further interest in the band structures and physical properties of the compounds.

2. Experimental

Material synthesis

The compounds were prepared using a solid-state high pressure synthesis method. Stoichiometric elementary iridium (Alfa Aesar 99.9%) or rhodium powders (Alfa Aesar 99.95%), tellurium pieces (Alfa Aesar 99.9999%), and iodine (Alfa Aesar 99.99 + %, resublimed for purification) were pre-mixed and loaded in a boron nitride crucible. The assembly was then inserted into a pyrophillite cube and pressed to a pressure of 6 GPa with a cubic multi-anvil system (Rockland Research Corporation). After the pressure was applied, the material was heated to 800–900 °C at 50 °C min⁻¹ and held at the desired temperature for 1 hour. The temperature was determined by an internal thermocouple. The system was quench-cooled before depressurizing, and small crystals found in the post-reaction polycrystalline products were saved for single crystal X-ray diffraction (SXRD) measurements.

Crystal structure determination

Multiple IrTe₂I and RhTe₂I crystals (\sim 80 \times 80 \times 15 μ m³), cleaved from as-made samples, were studied by SXRD to deter-

^aDepartment of Chemistry, Princeton University, Princeton, NJ 08544, USA. E-mail: rcava@princeton.edu

^bDepartment of Physics, Princeton University, Princeton, NJ 08544, USA

^cDepartment of Chemistry and Chemical Biology, Rutgers University, Piscataway, NJ 08854. USA

[†]Electronic supplementary information (ESI) available. See DOI: https://doi.org/ 10.1039/d2dt01224c

Dalton Transactions

mine the crystal structure. The structure, consistent among all crystals, was determined using a Bruker D8 QUEST diffractometer equipped with APEX III software and Mo radiation $(\lambda_{Ka} = 0.71073 \text{ Å})$ at room temperature. The crystals were mounted on a Kapton loop. Data acquisition was made via the Bruker SMART software with corrections for Lorentz and polarization effects included. A numerical absorption correction based on crystal-face-indexing was applied through the use of XPREP. The direct method and full-matrix least-squares on F^2 procedures within the SHELXTL package were employed to solve the crystal structure. 24,25 The SXRD data for RhTe₂I were successfully collected and refined, while the IrTe2I samples were too polycrystalline to generate high-quality single crystal diffraction data. Thus laboratory powder X-ray diffraction (PXRD) patterns were collected on a Bruker D8 Advance Eco diffractometer with Cu K α radiation ($\lambda = 1.5418 \text{ Å}$) to quantitatively determine its structure. A Rietveld refinement using GSAS II software was conducted on the PXRD data from polycrystalline IrTe₂I, and a preliminary structure was obtained. (In such refinements the thermal parameters for the atoms have no detailed meaning aside from indicating that the structure solution is well-behaved.) A Le Bail fit of RhTe2I PXRD pattern was carried out via the TOPAS software to confirm the uniformity of the bulk material.

Property characterization

The temperature-dependent and field-dependent magnetization (M) data were collected on a Quantum Design (QD) Physical Property Measurement System (PPMS), using an ACMS option. The magnetic susceptibility was defined as M/H. Electrical transport measurements were carried out on QD PPMS Dynacool, with phosphor bronze wires (for IrTe2I) and platinum wires (for RhTe2I) attached to samples using silver paint. No indication of reaction of the silver paint with the sample was observed during the measurements.

Magnetoresistance measurements were conducted on IrTe2I polycrystalline pieces at applied magnetic fields up to 9 T. A Keithley 2400 Source was used to perform two-probe resistivity measurements in the constant voltage (V) mode. The sample resistance is therefore given by R = V/I.

The diffuse reflectance data were collected at ambient temperature on a Cary 5000i UV-VIS-NIR spectrometer with an internal DRA-2500 integrating sphere. The reflectance data were transferred to pseudo absorbance using Kubelka-Munk theory and the band gap values were calculated from the Tauc plots.26

Electronic structure calculation

Density Functional Theory (DFT) calculations with the projector augmented-wave (PAW)²⁷ method were performed using the Vienna Ab initio Simulation Package (VASP)²⁸ version 5.4.4. The generalized gradient approximation (GGA) parameterized Perdew-Burke-Ernzerhof (PBE) functional²⁹ was used to account for the electronic exchange and correlation. A kinetic energy cutoff of 400 eV was used for the plane-wave basis set. Γ -Point centered Monkhorst-Pack³⁰ k-point grids of 8 × 4 × 8

and $12 \times 6 \times 12$ were applied to sample the Brillouin zone for the self-consistent field calculation and density of states (DOS), respectively. Spin-orbit coupling (SOC) was included in the calculations once specified. The structures were relaxed until the maximum absolute total force on each atom was smaller than 10^{-3} eV Å^{-1} and the energy converged to 10^{-8} eV.

Results and discussion 3.

Samples of IrTe₂I and RhTe₂I were prepared by solid-state high-pressure synthesis. High yields were obtained for both compounds through one-hour annealing at 800 °C and 6 GPa. No oxidic impurities were observed in either sample, however a small amount of RhTe2 was found as an impurity in the post-reaction RhTe₂I product. This small amount of impurity could not be eliminated when 10% excess iodine was used under the same conditions. The compounds are isostructural, with an orthorhombic unit cell in the non-centrosymmetric non-symmorphic space group $Pca2_1$. (IrTe₂I: a = 6.362 Å, b =10.57 Å, c = 6.405 Å, Z = 4; RhTe₂I: a = 6.368 Å, b = 10.56 Å, c =6.416 Å, Z = 4), which is exhibited in Fig. 1. (In other words, there is no inversion center in their structures, and no point that can be defined such that all symmetries present are the product of a symmetry that fixes this point plus a lattice translation.) Both non-centrosymmetric and non-symmorphic crystal structures have been postulated to give rise to topological physics, 31,32 but the study of topological properties is not the aim of the current research. These two compounds can't be formed using the solid-state preparation method at ambient pressure, and their refined structure is quite different

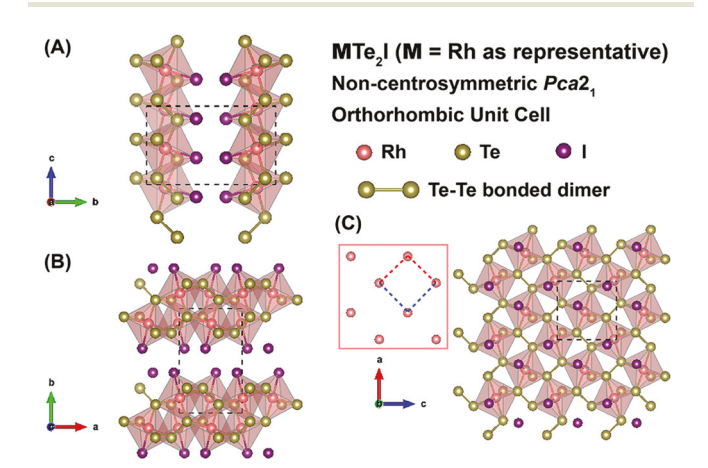


Fig. 1 The non-centrosymmetric crystal structures of high-pressuresynthesized IrTe₂I and RhTe₂I with the structure of RhTe₂I presented in this figure as the representative of the two isostructural compounds. Views along the (A) a-axis, (B) c-axis, and (C) the layer stacking direction b-axis are exhibited respectively. Te-Te bonded dimers can be clearly observed through the different views of the structure. The inset in (C) reveals the in-plane arrangement of metal cation lattice, with M-M distance at 4.40 Å (red dashed line, shorter) and 4.64 Å (blue dashed line, longer) in RhTe₂I. These distances are 4.39 Å and 4.64 Å respectively

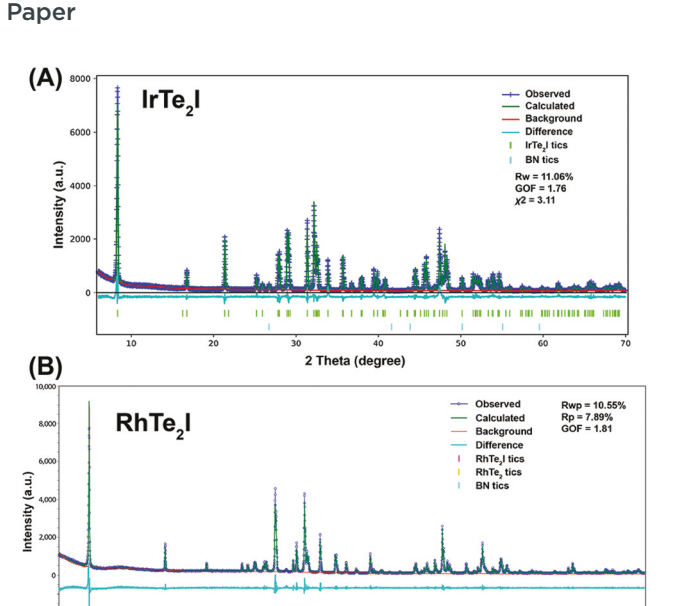


Fig. 2 Ambient temperature powder X-ray diffraction data for the two materials. (A) Rietveld refinement of the laboratory PXRD pattern of IrTe₂I; (B) Le Bail fit of the laboratory PXRD pattern of RhTe₂I. A small amount of RhTe2 is found as an impurity in the RhTe2l product.

2 Theta (degree)

from other reported ternary M-Te-I phases, which are generally coordination polymers or molecular clusters. 33,34 The powder diffraction pattern of IrTe₂I is shown in Fig. 2A and its crystallographic information is listed in Table 1. The crystal structure of RhTe2I was refined by SXRD (Tables 2-4), and Le Bail fitting performed on the PXRD data from the full as-synthesized sample confirms the bulk uniformity (Fig. 2B).

The materials have a layered structure, made from MTe₅I (M = Ir or Rh) octahedra connected by sharing corners. Revealed by the view along the *c*-axis, it is observed that these layers are double-tiered, through sharing vertices of the octahedra (Fig. 1B), with iodine mediated van der Waals interactions between the layers. The layers stack along the b-axis of the orthorhombic unit cell, leading to a strong (010) peak at low angle in their PXRD patterns (which can be observed in Fig. 2).

Table 2 Single crystal structure refinement for RhTe2I at 293(2) K. Standard deviations are presented in the brackets

Refined formula	RhTe₂I
Temperature (K)	293 (2)
F.W. $(g \text{ mol}^{-1})$	485.01
Space group; Z	$Pca2_1; 4$
a (Å)	6.368(1)
b(A)	10.562(2)
$c(\mathring{A})$	6.416(1)
$V(\mathring{A}^3)$	431.5(2)
θ range (°)	3.736-31.476
No. reflections; $R_{\rm int}$	6055; 0.0322
No. independent reflections	1425
No. parameters	15
R_1 : w R_2 $(I > 2\sigma(I))$	0.0341; 0.0687
Goodness of fit	1.354
Diffraction peak and hole (e ⁻ Å ⁻³)	2.038; -1.986
Flack parameter	0.40(11)

Table 3 Standardized atomic coordinates and equivalent isotropic displacement parameters for RhTe₂I at 293(2) K. ($U_{\rm eq}$ is defined as onethird of the trace of the orthogonalized U_{ii} tensor ($Å^2$)) standard deviations are presented in the brackets

Atom	Wyck.	Occ.	x	у	z	$U_{ m eq}$
Rh	4 <i>a</i>	1	0.0135(2)	0.1449(1)	0.0000	0.0079(2)
Te1	4 <i>a</i>	1	0.6265(1)	0.0804(1)	0.1193(1)	0.0088(2)
Te2	4 <i>a</i>	1	0.1232(1)	0.2366(1)	0.3634(1)	0.0099(2)
Ir	4 <i>a</i>	1	0.0834(2)	0.6162(1)	0.3812(2)	0.0164(2)

The view along the b axis in Fig. 1C shows that this structure can be considered as resembling a deformed section of the pyrite structural type, as the MTe₅I octahedra form a distorted triangular arrangement of metal cations that is close to being a square net (Fig. 1C inset). This layered structure in the noncentrosymmetric, non-symmorphic Pca21 space group thus may attract potential interest, as it can serve as a breeding ground for several potentially interesting properties such as ferroelectricity. The MTe₅I coordination octahedra are slightly distorted for both compounds (especially when compared to the symmetric octahedral coordination environment of CdI2type IrTe₂ with $d_{\text{Ir-Te}} = 2.65 \text{ Å},^{35}$ and pyrite type RhTe₂ with $d_{\rm Rh-Te}$ = 2.65 Å (ref. 36)), and the bond lengths between central

Table 1 Structural parameters and standardized crystallographic positions of IrTe21, from the Rietveld refinement of laboratory powder X-ray diffraction data collected at 300 K. Standard deviations are presented in the brackets

Refined formula F.W. (g mol ⁻¹) Space group; Z a (Å) b (Å) c (Å) V (Å 3)				IrTe ₂ I 574.32 Pca2 ₁ ; 4 6.36195(15) 10.57425(24) 6.40453(15) 430.851(27)		
Atom	Wyck.	Occ.	x	у	z	$U_{\rm iso}$ equiv. $[\mathring{\text{A}}^2]$
Ir	4 <i>a</i>	1	0.0141(4)	0.1418(2)	0.0000	0.0050(8)
Te1	4a	1	0.6238(6)	0.0829(3)	0.1170(4)	0.0041(14)
Te2	4a	1	0.1221(6)	0.2341(3)	0.3646(5)	0.0060(13)

0.6185(3)

0.0885(5)

0.0233(15)

0.3833(4)

Table 4 Anisotropic thermal displacement parameters for RhTe₂I at 293(2) K.^a Standard deviations are presented in the brackets

Atom	U_{11}	U_{22}	U_{33}	U_{12}	U_{13}	U_{23}
Rh	0.0064(4)	0.0108(4)	0.0063(3)	-0.0005(4)	0.0003(4)	0.0002(3)
Te1	0.0063(3)	0.0126(4)	0.0075(3)	0.0010(3)	0.0010(3)	0.0008(3)
Te2	0.0084(3)	0.0136(4)	0.0077(3)	0.0002(3)	0.0004(4)	0.0002(3)
I	0.0176(4)	0.0145(4)	0.0172(4)	-0.0024(4)	0.0015(4)	0.0030(3)

^a For an explanation of the anisotropic thermal displacement parameters, see *The International Tables for Crystallography*, ed. A. Authier, John Wiley and Sons, 2014, 2nd edn, vol. D, pp. 231–245.⁴¹

Table 5 Selected bond lengths (Å) for MTe_2l with M = Ir or Rh. Standard deviations are presented in the brackets

Dalton Transactions

Bonds	$IrTe_2I$	$RhTe_2I$
М-Те	2.587(4)	2.6012(15)
	2.622(5)	2.6198(16)
	2.657(5)	2.6570(15)
	2.668(5)	2.6685(15)
	2.679(4)	2.6877(16)
M-I	2.721(4)	2.7073(16)
Те-Те	2.760(5)	2.8187(13)

cations and the anions are listed in Table 5. The values of these distances are fairly close when comparing Ir and Rh, suggesting comparable M–X (X = Te or I) bond strengths in the two systems. All of the tellurium atoms are found to be covalently bonded so as to form Te–Te dumbbells in both compounds, with a relatively short Te–Te distance at 2.76 Å in IrTe₂I and 2.82 Å in RhTe₂I (as a comparison, the shortest Te–Te distance is around 2.83 Å in Ir₃Te₈, 3.08 Å in pyrite RhTe₂, and 2.77 Å in BaTe₂ $^{36-38}$). This chalcogen dimerization phenomenon is also observed in some other chalcogenide compounds $^{38-40}$ resulting in an average chemical valence of $^{-1}$ for Te in the MTe₂I formula, and thus a +3 valence with d^6

electronic configuration for both Ir and Rh. The shortest M–M in-plane distance is 4.39 Å for Ir, and 4.40 Å for Rh (Fig. 1C inset), and the distance between the two layers is 7.57 Å for Ir and 7.50 Å for Rh, thus it can be seen that IrTe₂I and RhTe₂I have very similar lattice dimensions and interatomic separations. The minor differences may be due to the slight difference between the Ir and Rh atomic radii and electronegativities, which may in turn be attributed to lanthanoid contraction in the sixth row of the periodic table. There is a shorter Te–Te distance and larger interplane spacing in IrTe₂I, which suggests stronger bonding of the ditelluride dimer in the system, and weaker interaction between the layers when compared to the Rh variant.

Temperature- and field-dependent magnetization measurements were carried out on the polycrystalline powders of $IrTe_2I$ and $RhTe_2I$. Both compounds show diamagnetic behavior, as shown in Fig. 3A, as their magnetic susceptibilities are negative under an applied filed of 0.1 T from 1.8 to 300 K. Both materials display a small upturn in susceptibility below 10 K, which we attribute to the presence of very small amounts of paramagnetic impurities. The observed susceptibility is consistent with a low-spin d^6 electron configuration of the M(III) ions and supports the existence of the observed Te–Te bonding in the MTe₂I system. The magnetization decreases with

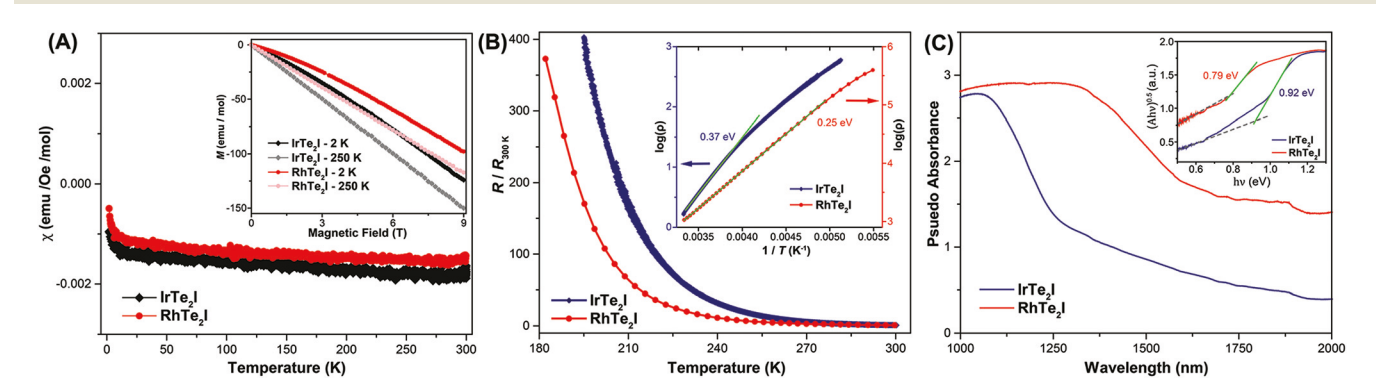


Fig. 3 Basic magnetic, electrical and optical absorption characterization of $IrTe_2I$ and $RhTe_2I$. (A) Temperature-dependent magnetic susceptibilities measured on polycrystalline powder samples from 1.8 to 300 K, with the inset presenting field-dependent magnetization measurements from 0 to 9 T at two different temperatures for each sample; (B) resistance measured from 180 to 300 K on as-made dense samples, where $R_{300 \text{ K}}$ represents the resistance at 300 K. The inset shows the $log(\rho)$ of both samples ($IrTe_2I$ on left y-axis and $RhTe_2I$ on right y-axis), plotted versus T^{-1} , with the linear fitting (green lines) on the higher temperature range of each curve employed to calculate the charge transport activation energy; (C) pseudo Kubelka-Munk absorbance spectra (main panel) and the Tauc plot for the indirect optical transitions (inset) for polycrystalline samples. The optical band gap values are estimated by extrapolating the intersection of the green lines (the linear absorption region) and the gray dashed lines (absorption baseline).

Paper Dalton Transactions

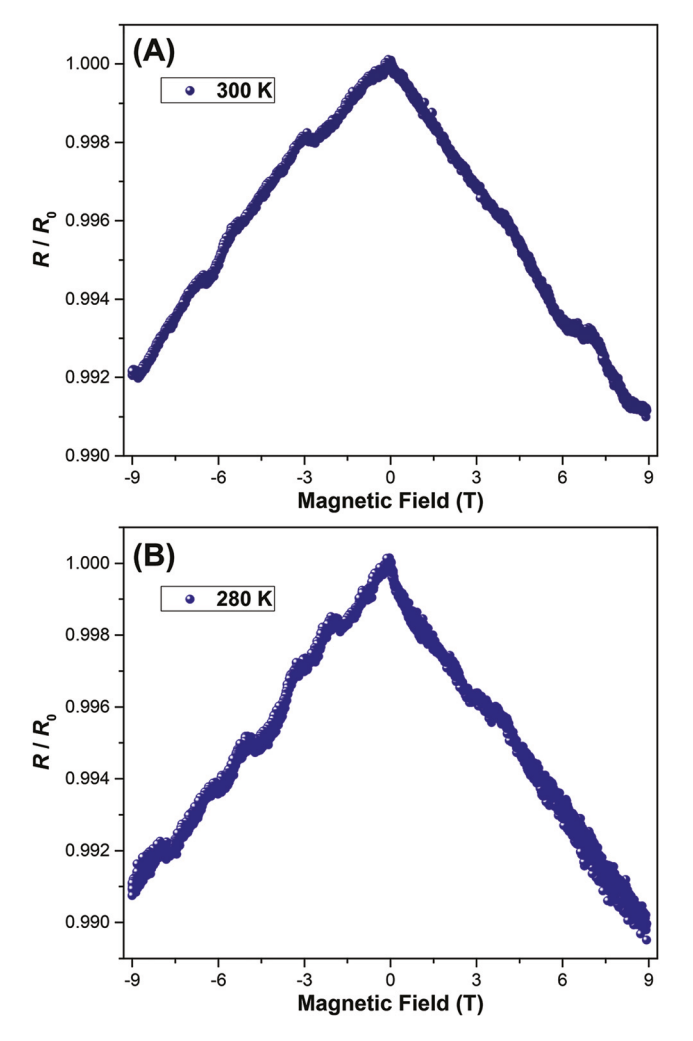


Fig. 4 Magnetoresistance measurements on a polycrystalline dense piece of $IrTe_2I$ at (A) 300 K and (B) 280 K, under an applied magnetic field swept from 9 T to -9 T. R_0 is the resistance under zero applied field. The excitation voltage is 5 V.

increasing magnetic field at both 2 K and 250 K for IrTe₂I and RhTe₂I (Fig. 3A inset), which is an indication of the diamagnetic nature of the materials.

Temperature dependent resistance measurements were also conducted on as-made dense pieces of the polycrystalline samples (Fig. 3B). Both compounds show semiconducting behavior, demonstrated by the fact that their resistivities increase with decreasing temperature until the measured values exceed the instrumental limits. $\text{Log}(\rho)$ for both samples is plotted *versus T*⁻¹ in the inset of Fig. 3B. The transport activation energies (E_a) for each compound near ambient temperature can be obtained by fitting the linearly varying parts of the curves to:

$$\rho = \rho_0 e^{-\frac{E_a}{k_B T}} \tag{1}$$

where ρ_0 is the pre-exponential term and $k_{\rm B}$ is Boltzmann's constant. The transport $E_{\rm a}$ s obtained are 0.37 eV for IrTe₂I and 0.25 eV for RhTe₂I. The semiconducting nature of the resistivity is consistent with the diffuse reflectance measurements shown in Fig. 3C.

The wavelength-dependent pseudo absorbance (*A*) data of IrTe₂I and RhTe₂I are presented, as are the Tauc plots for indirect transitions, shown in the inset. Using the equation:

$$Ah\nu = K(h\nu - E_{g})^{n} \tag{2}$$

for which n=0.5 for direct transitions and 2 for indirect transitions, and K is a constant, the indirect band gap value is calculated to be 0.92 eV for IrTe_2I and 0.79 eV for RhTe_2I . If instead the transitions are direct, the band gaps are 0.98 eV and 0.74 eV for M=Ir and K respectively, which, for present purposes, are not significantly different from the indirect case.

The magnetoresistance (MR) measurements were conducted on a polycrystalline dense sample of $IrTe_2I$ at different temperatures, and the R/R_0 values at 300 K and 280 K are plotted *versus* field in Fig. 4. (The slight asymmetry of the curves may be due to contributions from the Hall component.) A small negative MR effect of around 1% at 9 T is observed at

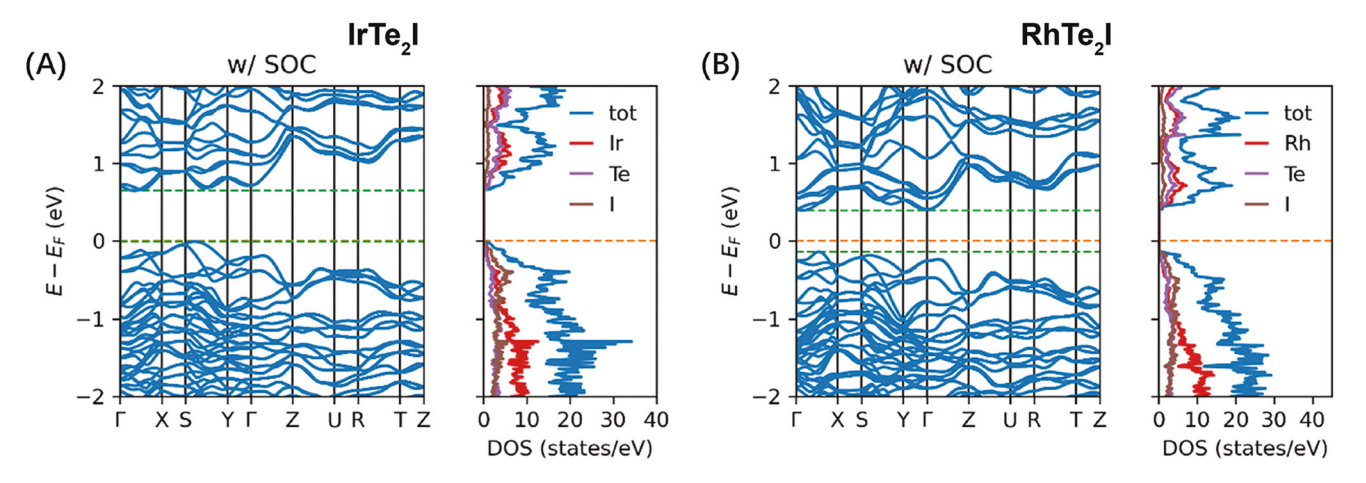


Fig. 5 The calculated electronic band structures and DOS for (A) $IrTe_2I$ and (B) $RhTe_2I$ with SOC included. Fermi level (E_F), conduction band minimum (CBM), and valence band maximum (VBM) are highlighted by orange dash lines and green dash lines.

Dalton Transactions Paper

room temperature. As negative MR effects generally originate from ferromagnetism or in metallic materials, it is surprising that this negative MR behavior is observed in diamagnetic semiconducting IrTe2I compound. One of the possible explanations is that the weak MR effect is induced by the strong spin orbit coupling (SOC) and non-centrosymmetric nature of the compound. This potential SOC induced MR will be further discussed during the description of the results of the theoretical calculations.

The electronic band structures and corresponding density of states for IrTe2I and RhTe2I, calculated without and with SOC included, are presented in Fig. 5 and S1.† The crystal structures were optimized prior to band structure calculations in order to find the lowest calculated energies. This optimization results in an increased unit cell size, an extended interlayer distance, and slightly lengthened bonds (especially the Te-Te bond) compared to the experimental structures, with the difference between the experimental and the optimized structures shown in Fig. S2.† The hybridization of the d-orbitals of the metals with the s and p orbitals from I and Te dominates the electronic states near E_F in both cases. IrTe₂I and RhTe2I are both calculated to be indirect gap semiconductors with band gaps of 0.66 eV and 0.53 eV, respectively. Consistent with the experimentally measured results, the Ir variant has a larger band gap value. The band gap in the Γ -X-S-Y- Γ region of the Brillouin zone is significantly smaller than the band gap in the Z-U-R-T-Z region, an indication of the stronger intralayer interactions (Γ -X-S-Y- Γ) in the structure. After including SOC in the calculation, the bands split significantly, reducing the calculated band gaps by about ~0.2 eV. The notable change when adding SOC in the calculation also suggests that the strong effect of SOC may be able to induce some unconventional properties, such as the weak negative MR behavior mentioned previously.

Summary and conclusion

The previously unreported compounds IrTe2I and RhTe2I were synthesized using a solid-state high-pressure method. Their structures were refined by SXRD and laboratory PXRD data, and found to be layered, with an orthorhombic unit cell in the non-centrosymmetric, non-symmorphic space group Pca2₁. Te-Te bonded dimers are seen, leading to a +3 chemical valence with d^6 electronic configuration of the metal cations, consistent with the diamagnetic, highly resistive behavior of the two compounds. The semiconducting nature of both compounds is revealed by experimental resistance, diffuse reflectance measurements and theoretical calculations. A weak negative MR effect is observed for IrTe2I, which may be induced by its strong SOC. This MR effect may be of future research interest, and this newly discovered non-centrosymmetric, non-symmorphic layered structure type may inspire future experimental and theoretical exploration and developments in material fabrication and applications of heavy transition metal compounds.

Conflicts of interest

The authors declare no conflict of interest.

Acknowledgements

This research was funded by the Gordon and Betty Moore foundation, EPiQS initiative, grant GBMF-9066, by the MRSEC award from NSF Grant DMR 2011750, and by the Arnold and Mabel Beckman Foundation through a Beckman Young Investigator Award to W. X. The single crystal diffraction work at Rutgers University was supported by the U.S. DOE-BES under Contract DE-SC0022156.

References

- 1 M. S. Dresselhaus, G. Chen, M. Y. Tang, R. G. Yang, H. Lee, D. Z. Wang, Z. F. Ren, J.-P. Fleurial and P. Gogna, New Directions for Low-Dimensional Thermoelectric Materials, Adv. Mater., 2007, 19, 1043-1053.
- 2 M. Guch, C. Raj Sankar, J. R. Salvador, G. P. Meisner and H. Kleinke, Improvements of the thermoelectric properties of PbTe via simultaneous doping with indium and iodine, J. Appl. Phys., 2012, 111, 063706.
- 3 A. Yamashita, Y. Goto, A. Miura, C. Moriyoshi, Y. Kuroiwa and Y. Mizuguchi, n-Type thermoelectric metal chalcogenide (Ag,Pb,Bi)(S,Se,Te) designed by multi-site-type highentropy alloying, Mater. Res. Lett., 2021, 9, 366-372.
- 4 B. M. Başol and B. McCandless, Brief review of cadmium telluride-based photovoltaic technologies, J. Photonics Energy, 2014, 4, 040996.
- 5 A. Singh, K. M. Boopathi, A. Mohapatra, Y. F. Chen, G. Li and C. W. Chu, Photovoltaic Performance of Vapor-Assisted Solution-Processed Layer Polymorph of Cs₃Sb₂I₉, ACS Appl. Mater. Interfaces, 2018, 10, 2566-2573.
- 6 G. Chen, Y. Yu, K. Zheng, T. Ding, W. Wang, Y. Jiang and Q. Yang, Fabrication of Ultrathin Bi₂S₃ Nanosheets for High-Performance, Flexible, Visible-NIR Photodetectors, Small, 2015, 11, 2848-2855.
- 7 H. Wang, G. Chen, J. Xu, Y. Xu and Q. Yang, Effective Synthesis of Pb5S2I6 Crystals at Low Temperature for Fabrication of a High Performance Photodetector, Cryst. Growth Des., 2018, 18, 1987-1994.
- 8 H. L. Zhuang, V. R. Cooper, H. Xu, P. Ganesh, R. G. Hennig and P. R. C. Kent, Rashba effect in single-layer antimony telluroiodide SbTeI, Phys. Rev. B: Condens. Matter Mater. Phys., 2015, 92, 115302.
- 9 R. Yadav, N. A. Bogdanov, V. M. Katukuri, S. Nishimoto, J. van den Brink and L. Hozoi, Kitaev exchange and fieldinduced quantum spin-liquid states in honeycomb α-RuCl₃, Sci. Rep., 2016, 6, 37925.
- 10 X. Y. Pu, K. Zhao, Y. Liu, Z. T. Wei, R. Jin, X. S. Yang and Y. Zhao, Structural and transport properties of iridium-

Paper

doped Bi₂Se₃ topological insulator crystals, J. Alloys

Compd., 2017, 694, 272–275.
H. Okazaki, K. Terashima, D. Billington, K. Iwata,
T. Wakita, M. Tanaka, Y. Takano, Y. Muraoka and
T. Yokoya, Change in the electronic structure of the

bismuth chalcogenide superconductor CsBi_{4-x}Pb_xTe₆ by

dissociation of the bismuth dimers, J. Phys.: Condens.

12 K. F. Mak, K. He, C. Lee, G. H. Lee, J. Hone, T. F. Heinz and J. Shan, Tightly bound trions in monolayer MoS₂, *Nat. Mater.*, 2013, **12**, 207–211.

Matter, 2020, 32, 145501.

- 13 M. A. McGuire, Crystal and Magnetic Structures in Layered, Transition Metal Dihalides and Trihalides, *Crystals*, 2017, 7, 121.
- 14 T. Kong, K. Stolze, E. I. Timmons, J. Tao, D. Ni, S. Guo, Z. Yang, R. Prozorov and R. J. Cava, VI3—a New Layered Ferromagnetic Semiconductor, *Adv. Mater.*, 2019, 31, 1808074.
- 15 D. Ni, X. Gui, K. M. Powderly and R. J. Cava, Honeycomb-Structure RuI₃, A New Quantum Material Related to α-RuCl₃, Adv. Mater., 2022, 34, 2106831.
- 16 Y. Qi, S. Matsuishi, J. Guo, H. Mizoguchi and H. Hosono, Superconductivity in Defective Pyrite-Type Iridium Chalcogenides IrxCh₂ (Ch = Se and Te), *Phys. Rev. Lett.*, 2012, 109, 217002.
- 17 B. Rasche, A. Isaeva, A. Gerisch, M. Kaiser, W. Van den Broek, C. T. Koch, U. Kaiser and M. Ruck, Crystal Growth and Real Structure Effects of the First Weak 3D Stacked Topological Insulator Bi₁₄Rh₃I₉, *Chem. Mater.*, 2013, 25, 2359–2364.
- 18 S.-H. Baek, S.-H. Do, K.-Y. Choi, Y. S. Kwon, A. U. B. Wolter, S. Nishimoto, J. van den Brink and B. Büchner, Evidence for a Field-Induced Quantum Spin Liquid in α-RuCl₃, *Phys. Rev. Lett.*, 2017, 119, 037201.
- 19 Y. Imai, K. Nawa, Y. Shimizu, W. Yamada, H. Fujihara, T. Aoyama, R. Takahashi, D. Okuyama, T. Ohashi, M. Hagihala, S. Torii, D. Morikawa, M. Terauchi, T. Kawamata, M. Kato, H. Gotou, M. Itoh, T. J. Sato and K. Ohgushi, Zigzag magnetic order in the Kitaev spinliquid candidate material RuBr₃ with a honeycomb lattice, *Phys. Rev. B*, 2022, **105**, L041112.
- 20 J. V. Badding, High-pressure synthesis, characterization, and tuning of solid state materials, *Annu. Rev. Mater. Sci.*, 1998, 28, 631–658.
- 21 H. Hegger, C. Petrovic, E. G. Moshopoulou, M. F. Hundley, J. L. Sarrao, Z. Fisk and J. D. Thompson, Pressure-Induced Superconductivity in Quasi-2D CeRhIn₅, *Phys. Rev. Lett.*, 2000, 84, 4986–4989.
- 22 L. Yang, Y. Zhang, J. Wang, Y. Wang and W. W. Yu, Pressure-induced phase transitions of lead iodide, *RSC Adv.*, 2016, **6**, 84604–84609.
- 23 D. Ni, S. Guo, K. M. Powderly, R. Zhong and R. J. Cava, A high-pressure phase with a non-centrosymmetric crystal structure in the PbSe-PbBr₂ system, *J. Solid State Chem.*, 2019, 280, 120982.
- 24 G. M. Sheldrick, Crystal structure refinement with SHELXL, *Acta Crystallogr., Sect. C: Struct. Chem.*, 2015, **71**, 3–8.

- 25 N. Walker and D. Stuart, An empirical method for correcting diffractometer data for absorption effects, *Acta Crystallogr.*, Sect. A: Found. Crystallogr., 1983, 39, 158–166.
- 26 J. Tauc, R. Grigorovici and A. Vancu, Optical Properties and Electronic Structure of Amorphous Germanium, *Phys. Status Solidi B*, 1966, 15, 627–637.
- 27 P. E. Blöchl, Projector augmented-wave method, *Phys. Rev. B: Condens. Matter Mater. Phys.*, 1994, **50**, 17953–17979.
- 28 G. Kresse and J. Furthmüller, Efficiency of ab initio total energy calculations for metals and semiconductors using a plane-wave basis set, *Comput. Mater. Sci.*, 1996, **6**, 15–50.
- 29 J. P. Perdew, K. Burke and M. Ernzerhof, Generalized Gradient Approximation Made Simple, *Phys. Rev. Lett.*, 1996, 77, 3865–3868.
- 30 H. J. Monkhorst and J. D. Pack, Special points for Brillouinzone integrations, *Phys. Rev. B: Solid State*, 1976, **13**, 5188– 5192.
- 31 J. Liu and D. Vanderbilt, Weyl semimetals from noncentrosymmetric topological insulators, *Phys. Rev. B: Condens. Matter Mater. Phys.*, 2014, **90**, 155316.
- 32 J. Cano, B. Bradlyn, Z. Wang, L. Elcoro, M. G. Vergniory, C. Felser, M. I. Aroyo and B. A. Bernevig, Topology of Disconnected Elementary Band Representations, *Phys. Rev. Lett.*, 2018, 120, 266401.
- 33 A. Günther and M. Ruck, Hexatellurium Rings in Coordination Polymers and Molecular Clusters: Synthesis and Crystal Structures of [M(Te₆)]X₃ (M = Rh, Ir; X = Cl, Br, I) and [Ru₂(Te₆)](TeBr₃)₄(TeBr₂)₂, *Z. Anorg. Allg. Chem.*, 2012, **638**, 317–323.
- 34 A. Günther, A. Isaeva and M. Ruck, Stabilization of Decatellurium Molecules in Isolated and Concatenated Clusters, *Z. Anorg. Allg. Chem.*, 2013, **639**, 254–260.
- 35 S. Jobic, P. Deniard, R. Brec, J. Rouxel, A. Jouanneaux and A. N. Fitch, Crystal and electronic band structure of IrTe₂: Evidence of anionic bonds in a CdI₂-like arrangement, *Z. Anorg. Allg. Chem.*, 1991, **598**, 199–215.
- 36 S. Geller, The Crystal Structures of RhTe and RhTe₂, *J. Am. Chem. Soc.*, 1955, 77, 2641–2644.
- 37 S. Jobic, M. Evain, R. Brec, P. Deniard, A. Jouanneaux and J. Rouxel, Crystal structure of polymeric pyrite type Ir₃Te₈, *J. Solid State Chem.*, 1991, **95**, 319–326.
- 38 J. Li, H.-Y. Guo, J. R. Carey, S. Mulley, D. M. Proserpio and A. Sironi, Synthesis and crystal structure of a new alkaline-earth metal chalcogenide: Barium ditelluride, *Mater. Res. Bull.*, 1994, **29**, 1041–1048.
- 39 M. Bremholm, Y. S. Hor and R. J. Cava, Pressure stabilized Se–Se dimer formation in PbSe₂, *Solid State Sci.*, 2011, 13, 38–41.
- 40 D. Ni, S. Guo, K. M. Powderly, R. Zhong, J. Lin, T. Kong, F. Alex Cevallos and R. J. Cava, Crystal structure and elementary properties of PbS₂ with a pressure–stabilized S-S dimer, *J. Solid State Chem.*, 2019, 269, 442–446.
- 41 International Tables for Crystallography, Physical Properties of Crystals: Physical Properties of Crystals, ed. A. Authier, John Wiley and Sons, 2nd edn, 2014, vol. D.